PHYSICAL REVIEW B VOLUME 15, NUMBER 4 15 FEBRUARY 1977

LMM Auger spectra of Cu, Zn, Ga, and Ge. I. Transition probabilities, term splittings, and effective Coulomb interaction

E. Antonides, E. C. Janse, and G. A. Sawatzky
Laboratory of Physical Chemistry, Materials Science Center, University of Groningen, The Netherlands
(Received 21 May 1976)

The *LMM* Auger spectra of Cu, Zn, Ga, and Ge are presented and discussed. Transition probability calculations are described and with these a clear assignment of the peaks can be made. It is further shown that from the $L_3M_{45}M_{45}$ Auger lines the term splittings and the effective on-site electron-electron interaction can be determined. The latter is shown to be strongly reduced from the free-atom value. This has important consequences for the description of the band structure using one-electron theories. The satellite structure for Cu and Zn in the $L_3M_{45}M_{45}$ region of the spectrum is shown to be a result of strong Coster-Kronig processes involving the L_2 and L_3 core levels.

I. INTRODUCTION

High-resolution *LMM* Auger measurements of the transition metals are extremely important for an understanding of electron correlation effects in d-band metals. In a recent paper[1] we have discussed this in some detail. It will become clear that from the $L_3M_{45}M_{45}$ Auger spectra the effective Coulomb interaction U_{eff} between two $3d$ holes on the same site can be determined. U_{eff} is strongly reduced from the free-atom value because of electronic as well as lattice polarization effects. This reduction can in fact exceed the ordinary Coulomb interaction leading to the formation of "bipolarons." The relative magnitude of U_{eff} as compared to the one-electron valence bandwidth Γ is of utmost importance in a number of problems. It is well known from Hubbard's papers[2] that for $U_{\text{eff}} \gg \Gamma$ the material will behave like a strongly correlated metal for a less than half-filled nondegenerate band and for a nondegenerate half-filled band like a Mott-Hubbard insulator. For $U_{\text{eff}} \ll \Gamma$ the material will behave much like an ordinary metal. The one-electron bandwidth can be studied by x-ray photoelectron spectroscopy (XPS) and U_{eff} can be determined for $3d$ transition metals from the $L_3M_{45}M_{45}$ Auger lines.

Also for a description of transition-metal impurities in metals U_{eff} is a very important quantity. It, for example, appears in the Anderson Hamiltonian[3] describing virtual bound states and the appearance and size of localized magnetic moments. The size of the magnetic moments is also dependent on the exchange interactions. These can be determined from the term splittings of the $L_3M_{45}M_{45}$ Auger lines.

For the d-band structure and localized moments in $3d$ transition metals U_{eff} is also extremely important. For $U_{\text{eff}} \ll \Gamma$ one can justify a one-electron band-structure description. For $U_{\text{eff}} \gg \Gamma$ one must resort to models which include the on-site correlations as, for example, is done in the minimum polarity model.[4,5] In this model the charge on any particular site is not allowed to fluctuate by more than one electron.

Before dealing with the above theories one must have a detailed understanding of the various Auger processes and one must be able to make a clear assignment of the various peaks and satellite structure in these spectra. The purpose of this paper and a one to follow is to show that for Cu, Zn, Ga, and Ge in which the $3d$ states are full the Auger spectra can be understood in detail.

Since high-resolution *LMM* Auger spectra of transition metals have become available several papers have been published to account for absolute kinetic energies of the Auger electrons and multiplet structure. These results indicate that a satisfactory assignment can be made by considering the problem in an atomic rather than a solid-state way.[6-10] Absolute kinetic energies for the $L_{23}M_{45}M_{45}$ Auger electrons in Cu and Zn were calculated by Kowalczyk *et al.*[6] Their approach has very recently been improved by Hoogewijs *et al.*,[11] who introduced a hitherto neglected term in the extra-atomic relaxation energy. Recently detailed transition-probability calculations have been carried out for the $L_{23}MM$ Auger spectra of Se,[12] and for the $L_{23}M_{45}M_{45}$ Auger spectrum of Cu,[13] and atomic Zn.[14]

In this paper we have calculated the transition probabilities of all final-state terms in the $L_{23}M_{23}M_{23}$, $L_{23}M_{23}M_{45}$, and $L_{23}M_{45}M_{45}$ Auger processes in Cu, Zn, Ga, and Ge. We also determined U_{eff} and the term splittings for these materials. In the second paper we will give a detailed description of the satellite lines in the $L_3M_{45}M_{45}$ region of the Auger spectrum of Cu and

Zn and explain the $L_3M_{45}M_{45}$ to $L_2M_{45}M_{45}$ intensity ratios invoking a Coster-Kronig transition. As will be shown the intensity ratios can be determined from the L_2 and L_3 core-level widths in the XPS spectrum.

II. EXPERIMENTAL

The x-ray photoelectron and x-ray excited Auger spectra were collected with an AEI-ES 200 spectrometer using a Mg $K\alpha$ source with a linewidth of 0.7 eV. In one case (Ge) monochromatized Al $K\alpha$ radiation was used with a linewidth of about 0.4 eV. This was required for Ge because the Mg $K\alpha$ radiation is almost at the energy threshold for the Ge L_2 photoelectrons thereby decreasing the intensity ratio I_{L_2}/I_{L_3}. The use of the monochromator is the reason for the relatively bad signal to noise ratio in the Ge Auger lines. The spectra were obtained of foils clamped on a copper sample holder at temperatures of 20 °C for Cu, Zn, and Ge and 0 °C for Ga. The spectrometer was evacuated to better than 10^{-9} Torr and the data were collected with a PDP 8 computer. Before the spectra were taken the samples were cleaned by cycles of argon ion etching and heating, except for Ga which could not be heated because of its low melting point and therefore was cleaned by etching only. After this treatment the ratio of the heights of the O 1s and C 1s lines as compared to the L_3 lines was for all metals less than 3% and for Cu less than 1%. There also was no evidence of shoulders on the photoelectron lines indicating the absence of any oxidation. All spectra were corrected for the energy-dependent transmission of the analyzer and for scattered electrons. In the former correction the transmission of the analyzer including the retarding lens system is assumed to be inversely proportional to the kinetic energy of the electrons as has been derived by Helmer *et al.*[15] In the correction for the scattered electrons the probability (α) that a scattered electron suffers an energy loss is assumed to be independent of the amount of energy loss. Since the measurement is done at discreet points (E_i) in the energy distribution, we can write

$$I(E_n) = I^M(E_n) - \alpha \sum_{E_n}^{E_{\max}} I(E_i) .$$

Here $I(E_n)$ and $I^M(E_n)$ are the corrected and measured intensities at kinetic energy E_n and α is determined iteratively in a computer program developed for this purpose. $E_{\max}$ is the high energy cutoff of the spectrum. This procedure is similar to that mentioned very recently by Beatham *et al.*[16] The results of both corrections when executed on asymmetrically broadened photoelectron lines is quite satisfactory which gives us confidence to use them also for the Auger spectra. The importance of the corrections is displayed in Fig. 1 where the corrected as well as the uncorrected $L_{23}M_{23}M_{23}$ spectrum of Cu is shown as an example.

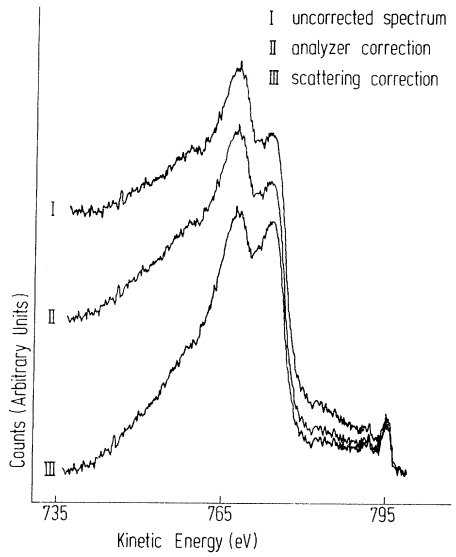

FIG. 1. Effect of the analyzer correction and the scattered electron correction on the $L_{23}M_{23}M_{23}$ Auger spectrum of Cu.

III. THEORY

The kinetic energy of LMM Auger electrons can be written[17]

$$E(L_aM_bM_c;X) = E(L_a) - E(M_b) - E(M_c) - \mathfrak{F}(M_bM_c;X) + R(M_bM_c;X) . \quad (1)$$

Here $E(L_a)$, $E(M_b)$, and $E(M_c)$ are the core-level binding energies which can be determined by XPS. $\mathfrak{F}(M_bM_c;X)$ describes the Coulomb energy of the holes created in the M_b and M_c levels. It is dependent on the final state term X of this two-hole configuration and can be expressed as the sum of Slater's direct and exchange integrals.[18] When spin-orbit interaction is considerable $\mathfrak{F}$ has to be calculated in the intermediate coupling scheme rather than in LS coupling. $R(M_bM_c;X)$, often called the total relaxation energy, is the additional relaxation energy due to the two-hole final state above and beyond the sum of the two one-hole relaxation energies. These latter values are included in $E(M_b)$ and $E(M_c)$. We can also lump the last two terms into one which is then a directly measured quantity

$$E(L_aM_bM_c;X) = E(L_a) - E(M_b) - E(M_c) - U_{\text{eff}}(M_bM_c;X) . \quad (2)$$

$U_{\text{eff}}(M_b M_c; X)$ is the total additional energy required to excite two holes M_b and M_c on the same atom for the final state term X above and beyond the two one-hole excitation energies. U_{eff} is then the effective Coulomb interaction of the two holes on one site reduced from the free-atom value by extra-atomic or band polarization. It should be noticed that we are at present not concerned with the various contributions to the relaxation energy which have been discussed by Hoogewijs *et al.*[11] but primarily with the effective two-hole Coulomb interaction.

Auger processes result from radiationless transitions that arise from the electrostatic interaction between two electrons in an atom initially singly ionized. The probability of such a transition is given by perturbation theory

$$\omega_{fi} = \left(\frac{2\pi}{\hbar}\right) \left| \int \phi^*_{f(X)} V \phi_i d\tau \right|^2 \rho(E_f) , \qquad (3)$$

where

$$V = \sum_{i \neq j} \frac{e^2}{r_{ij}}$$

and $\rho(E_f)$ is the density of final states for the energy E_f that satisfies conservation of energy. ϕ_i is the initial state consisting of one hole in an inner shell and one hole in the continuum. $\phi_{f(X)}$ is the two-hole final state term X in which the atom is left after the Auger process has taken place. The direct and exchange matrix elements occuring in Eq. (3) can be separated into radial and angular factors.[19] The calculation of these factors leads to the transition probability as a function of the final-state term X (see Appendix).

IV. RESULTS AND DISCUSSION

In Fig. 2 the three main parts of the *LMM* Auger spectra of Cu, Zn, Ga, and Ge are shown. There is a strong resemblance between the spectra of the different metals although certain differences can be noticed. One can see that the relative intensity of the L_2MM as compared to the L_3MM portion increases as one goes from Cu to Ga, having a value of about $\frac{1}{2}$ in the latter metal and staying approximately constant on going to Ge. The increase of the L_2/L_3 intensity ratio in the Auger spectra on going from Cu to Ga can be explained very satisfactory by considering a $L_2L_3M_{45}$ Coster-Kronig process, which has a decreasing probability on going from Cu to Ga because of the following. The necessary condition for this process to appear is that the L_3-L_2 energy difference must exceed the binding energy of the M_{45} electron, in the presence of the L_2 hole. This condition is easily satisfied for Cu. For Zn the M_{45} binding energy is close

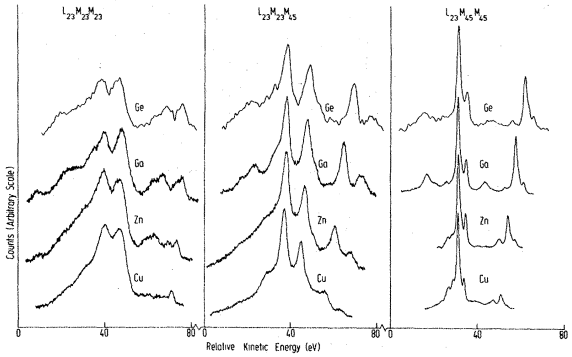

FIG. 2. Three main parts of the *LMM* Auger spectra of Cu, Zn, Ga, and Ge. The kinetic energy corresponding to the different metals has been shifted such that the most intense peaks come at the same position.

to threshold for this process.[20,21] For Ga and Ge the M_{45} binding energy is too large for the Coster-Kronig process to occur.[21] Therefore in Cu and Zn a fraction of the primarily created L_2 holes decays via this Coster-Kronig process, which in turn leads to a reduction in the L_2 part of the *LMM* Auger processes as compared to the L_3 part.

The satellites on the low-kinetic-energy side of the $L_3M_{45}M_{45}$ region which appear only in Cu and Zn can also be explained as being a result of the $L_2L_3M_{45}$ Coster-Kronig process.[13] After this process has taken place the created L_3 hole can decay via the normal $L_3M_{45}M_{45}$ Auger process, except that the initial state now already has a hole in the M_{45} level, created in the Coster-Kronig process. This means that the $L_3M_{45}M_{45}$ Auger process in this case ends up in a final state with three M_{45} holes instead of two M_{45} holes in the normal case. The difference between this Coster-Kronig preceded $L_3M_{45}M_{45}$ process and the common $L_3M_{45}M_{45}$ process gives rise to a shift to lower kinetic energy of the former one because of the Coulomb interaction between the Auger electrons and the extra M_{45} hole. A more detailed discussion of this subject including the effect of the $L_2L_3M_{45}$ Coster-Kronig process on the L_{23} photoelectron spectrum will be published in a second paper.

Aside from these differences all of the spectra exhibit several peaks which are a result of final state term splittings. The final states possible are ^1S, ^3P, ^1D, ^3F, and ^1G in the $L_{23}M_{45}M_{45}$ spectrum corresponding to two d holes. For the $L_{23}M_{23}M_{45}$ process the final-state terms are ^1P, ^3P, ^1D, ^3D, ^1F, and ^3F and for the $L_{23}M_{23}M_{23}$ process we find the terms ^1S, ^3P, and ^1D. In order to identify the peaks with the various final-state terms, transition probabilities are required. We calculated these in the j-j and LS coupling scheme

TABLE I. Calculated final-state term transition probabilities for Cu, Zn, Ga, and Ge. Absolute transition probabilities can be obtained by multiplying by $2\pi/(2j+1)$, where $2j+1$ is the multiplicity of the initial hole state. The multiplicities of the different final-state terms are indicated.

Auger process	Final-state term	Multiplicity	Transition probabilities (10^{-4} a.u.) Cu	Zn	Ga	Ge
$L_3M_{23}M_{23}$	^1S	1	4.51	4.34	4.95	5.03
	^1D	5	15.86	15.25	17.30	17.34
	^3P	9	18.57	17.82	20.47	20.21
$L_2M_{23}M_{23}$	^1S	1	2.25	2.17	2.47	2.52
	^1D	5	7.93	7.63	8.66	8.67
	^3P	9	9.29	8.91	10.24	10.11
$L_3M_{23}M_{45}$	^1F	7	13.09	13.60	15.20	16.81
	^1P	3	3.71	3.87	4.39	4.94
	^3D	15	7.74	8.04	8.99	9.96
	^3P	9	2.79	2.80	3.17	3.57
	^1D	5	0.33	0.32	0.35	0.38
	^3F	21	0.10	0.06	0.05	0.05
$L_2M_{23}M_{45}$	^1F	7	6.55	6.80	7.61	8.41
	^1P	3	1.86	1.93	2.19	2.47
	^3D	15	3.87	4.02	4.49	4.98
	^3P	9	1.39	1.40	1.58	1.78
	^1D	5	0.17	0.16	0.17	0.19
	^3F	21	0.05	0.03	0.03	0.02
$L_3M_{45}M_{45}$	^1S	1	1.15	1.26	1.60	1.94
	^1G	9	42.88	44.82	53.71	63.35
	^3P	9	1.37	1.51	1.92	2.34
	^1D	5	7.40	7.82	9.47	11.20
	^3F	21	16.18	16.88	20.25	23.99
$L_2M_{45}M_{45}$	^1S	1	0.58	0.63	0.80	0.97
	^1G	9	21.43	22.40	26.84	31.66
	^3P	9	0.69	0.76	0.96	1.17
	^1D	5	3.69	3.90	4.73	5.59
	^3F	21	8.10	8.46	10.14	12.02

for the initial and final state, respectively. The details are given in the Appendix. For the free-electron wave function we first tried plane waves but we were not able to get reasonable agreement with the spectra. We then resorted to radial integrals given by McGuire,[22] in which the free-electron wave function is modified close to the atom because of the interaction with the positive charge left behind. As will be discussed shortly these transition probabilities result in surprisingly good agreement with experiment. The calculated transition probabilities are given in Table I. The fact that the plane-wave functions are not at all satisfactory is interesting in itself. It shows that the interaction between the outgoing electron and the hole left behind even at kinetic energies of about 1000 eV is far from negligible. This is a strong indication that the sudden approximation usually used in XPS and Auger spectroscopy is probably not valid. It can be seen from the calculations given in Table I that there is little qualitative and certainly no quantitative relation between the transition probability and the multiplicity of the corresponding final-state term. The calculated transition probabilities of the final-state terms in the $L_3M_{45}M_{45}$ Auger process of Cu are in very good agreement with those obtained by Roberts *et al.*[13]

To display the excellent agreement between theory and experiment we show in more detail the $L_3M_{45}M_{45}$ spectrum of Ga in Fig. 3. For this metal there are no additional complications due to Coster-Kronig processes. We fitted this spectrum with the constraint that the intensity ratios of the terms were given by the theoretically calculated transition probabilities. The widths of the term peaks were constrained to be equal. The line shape of each peak was taken to be the sum of Lorentzian

TABLE II. Experimental and calculated atomic Coulomb integrals (eV) for the $L_{23}M_{45}M_{45}$ and $L_{23}M_{23}M_{23}$ Auger processes. See text.

Auger process	Coulomb integrals	Cu Expt.[a]	Cu Theor.[b]	Zn Expt.[a]	Zn Theor.[b]	Ga Expt.[a]	Ga Theor.[b]	Ge Expt.[a]	Ge Theor.[b]
$L_{23}M_{45}M_{45}$	F^2	10.0	11.65	13.0	13.30	14.8	14.88	16.2	16.36
	F^4	5.6	7.18	4.8	8.24	8.0	9.27	8.4	10.23
$L_{23}M_{23}M_{23}$	F^2	26.7	16.25	28.8	17.11	32.5	18.02	36.7	18.95

[a] From experimental peak splittings. [b] From Mann's table (Ref. 23).

and Gaussian character, with the ratio of Lorentzian to Gaussian left as a parameter in the fitting. The only other free parameters are the term splittings and positions which are determined by the Slater Coulomb and exchange integrals. The positions of the terms aside from a shift of the whole multiplet are given by[18] [see Eq. 1)]

$$
\begin{aligned}
-\mathfrak{F}(M_{45}M_{45};{}^1S) &= -F^0-\tfrac{2}{7}F^2-\tfrac{2}{7}F^4,\\
-\mathfrak{F}(M_{45}M_{45};{}^1G) &= -F^0-\tfrac{4}{49}F^2-\tfrac{1}{441}F^4,\\
-\mathfrak{F}(M_{45}M_{45};{}^3P) &= -F^0-\tfrac{1}{7}F^2+\tfrac{4}{21}F^4,\\
-\mathfrak{F}(M_{45}M_{45};{}^1D) &= -F^0+\tfrac{3}{49}F^2-\tfrac{4}{49}F^4,\\
-\mathfrak{F}(M_{45}M_{45};{}^3F) &= -F^0+\tfrac{8}{49}F^2+\tfrac{1}{49}F^4.
\end{aligned}
\qquad (4)
$$

From Eqs. (4) we see that the term splittings are determined by the F^2 and F^4 Coulomb integrals. The fit in Fig. 2 was determined by leaving F^2 and F^4 as free parameters. We see that the result of this fit is exceptionally good considering that the calculated intensities were used. It seems that the only significant deviation which occurs is that the theory predicts a slightly higher ${}^3F$ intensity (the peak on the high-kinetic-energy side of the spectrum) than is observed. From the fit we obtained widths of 1.4 eV for the various lines and a line shape with $\frac{2}{3}$ Lorentzian and $\frac{1}{3}$ Gaussian character. The values obtained for F^2 and F^4 for Cu, Zn, Ga, and Ge are given in Table II and are seen to be close to the free-atom values obtained from Mann,[23] except for the F^4 integrals of Cu and Zn. This is due to the fact that for these two metals the experimental F^2 and F^4 integrals were obtained from the $L_2M_{45}M_{45}$ Auger spectrum because of the pronounced influence of the $L_2L_3M_{45}$ Coster-Kronig process on the $L_3M_{45}M_{45}$ spectrum, as was mentioned before. In the $L_2M_{45}M_{45}$ spectrum of Cu and Zn we see that the ${}^1S$ final state has an anomalously high intensity. It is possible that for these metals the peak in the ${}^1S$ region originates from some other process, thereby causing a large uncertainty in the position of the real ${}^1S$ final state and therefore in the ${}^1S$-${}^1G$ term splitting. The experimental F^4 integral is mainly determined by this splitting, whereas the F^2 integral is mainly determined by the ${}^3F$-${}^1G$ term splitting [see Eqs. (4)].

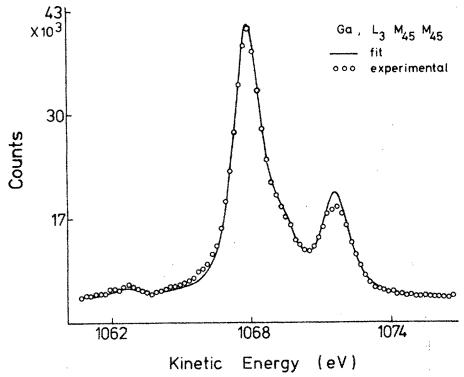

FIG. 3. Fit of the $L_3M_{45}M_{45}$ Auger spectrum of Ga to five lines corresponding to the five final-state terms ${}^1S$, ${}^1G$, ${}^3P$, ${}^1D$, and ${}^3F$, taking the F^2 and F^4 Coulomb integrals as free parameters. For details see text.

We now go on to discuss the positions and term splittings of the Cu, Zn, Ga, and Ge Auger spectra. As given by Eq. (2) the positions and splittings of the Auger lines are determined by the effective Coulomb interaction $U_{\text{eff}}(M_bM_c;X)$ and the binding energies $E(L_a)$, $E(M_b)$, and $E(M_c)$ as determined by XPS. The relevant binding energies we determined are given in Table III relative to the Fermi level. These are in good agreement with previously reported results.[6,24-26] In Figs. 4(a)–4(d) we show the Auger spectra in more detail. The solid and dashed bars display the calcu-

TABLE III. Experimental core-level binding energies (eV), relative to the Fermi level.

Level	Cu	Zn	Ga	Ge
L_2	952.0	1044.0	1142.9	1247.2
L_3	932.2	1020.9	1116.1	1216.2
M_1	122.5	139.6	158.9	180.9
M_2	77.2	91.0	106.9	125.2
M_3	75.2	88.4	103.8	121.4
M_{45}	3.1	9.9	18.4	29.2

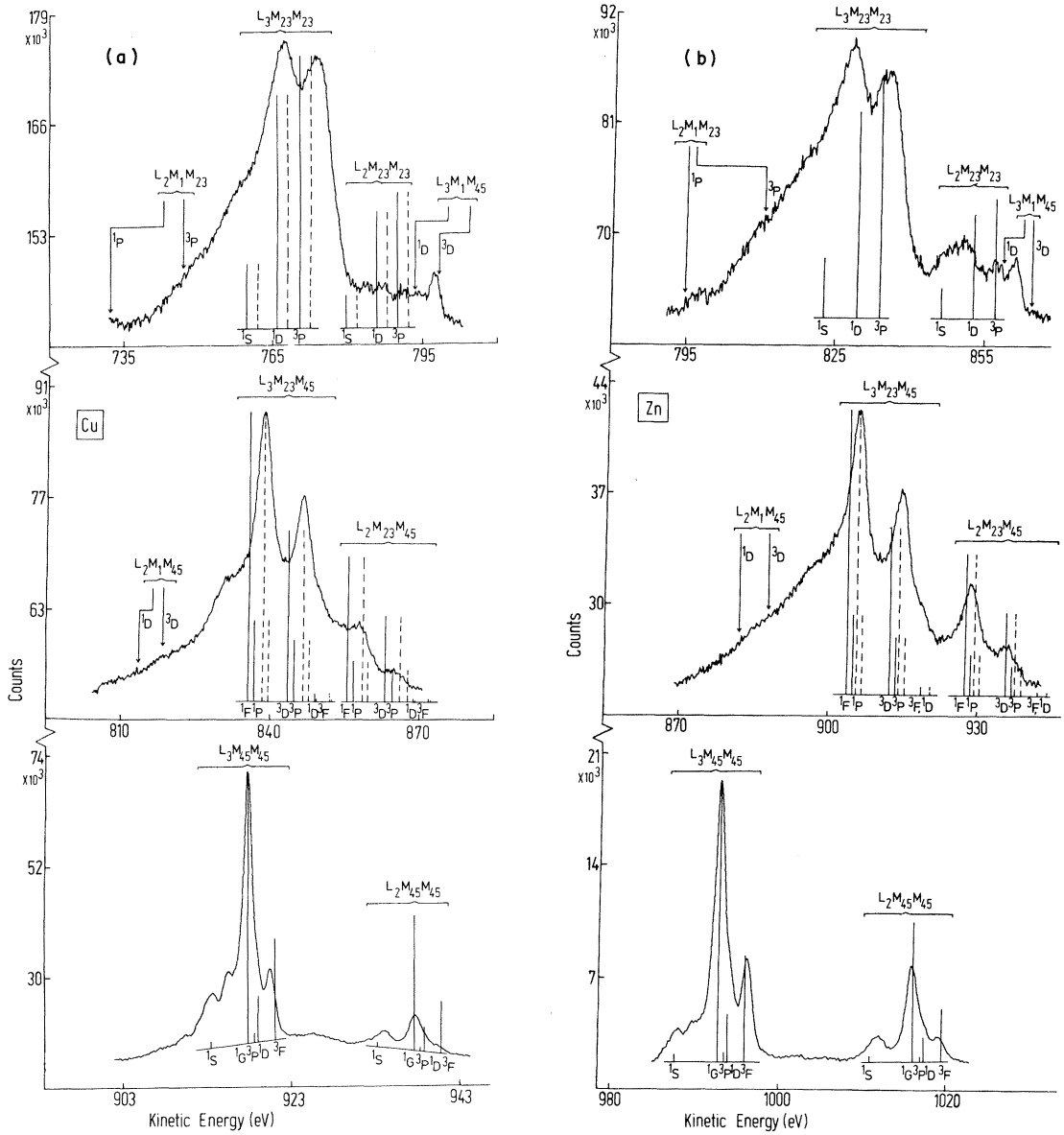

FIG. 4. Three main parts of the *LMM* Auger spectra of Cu, Zn, Ga, and Ge showing calculated transition probabilities. The solid and dashed lines are on positions obtained from two different approximations to the total relaxation energy R (see text). Those final-state terms that are split up by spin-orbit coupling are indicated on the average positions weighted by the multiplicities of the split terms. The positions of the most intense plasmon satellites and the Auger peaks involving the M_1 level are also indicated. These latter positions were obtained using $R(M_{45}M_{45};{}^1G)$ (Table IV). (a) Cu, (b) Zn, (c) Ga, (d) Ge.

lated intensities of the various terms and their positions based on two different approximations to $R(M_bM_c;X)$ in Eq. (1). For the solid lines we used calculated atomic values[23] for $\mathcal{F}(M_bM_c;X)$ (using Mann's integrals) and for R the value that was required to give the correct peak position for the ${}^1G$ term in the $L_3M_{45}M_{45}$ spectrum, assuming this value to be independent of M_b, M_c, and X. The values for $R(M_{45}M_{45};{}^1G)$ obtained in this way are given in Table IV. From Fig. 4 we see that the solid line positions agree fairly well with the experimental positions indicating that R is only weakly dependent on M_b, M_c, and X.[9,10] The dashed lines in Fig. 4 are obtained by again using atomic integrals for $\mathcal{F}(M_bM_c;X)$ and by taking $R(M_bM_c;X)$ to be independent of X but dependent on M_b and M_c. In this way slightly different values for R are obtained which are also listed in Table IV. We see

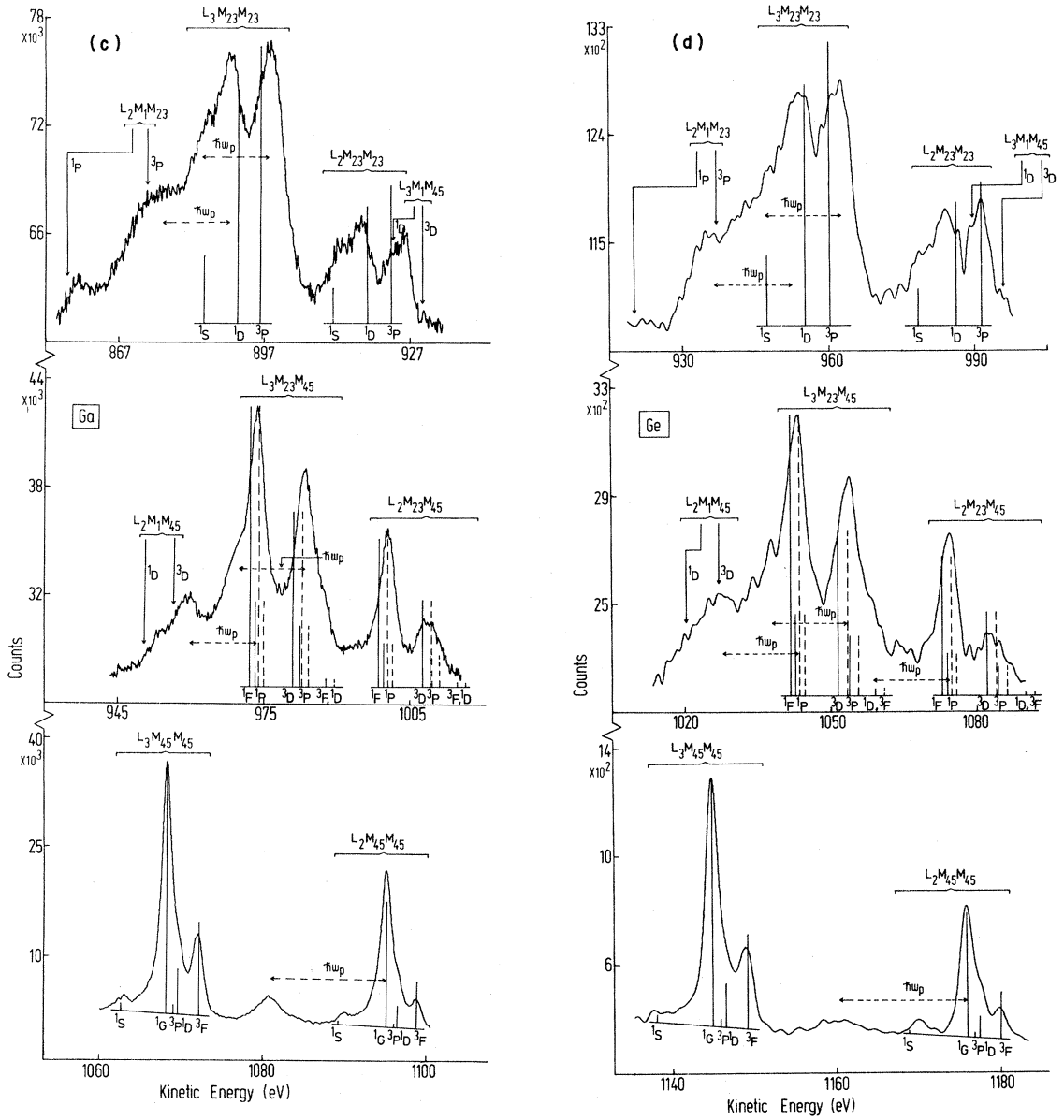

FIG. 4. (*Continued*)

indeed that R is only weakly dependent on M_b and M_c. These two ways of obtaining semiempirical peak positions are shown in Fig. 4 in order to display that there is no doubt as far as the assignment of the peaks are concerned. The experimental peak positions and their assignment are listed in Table V. Only those terms are shown for which an accurate determination could be made. The positions are in good agreement with values reported previously.[6,8,24,25]

Also indicated in Figs. 4(a)–4(d) are the positions of the most intense plasmon satellites for

TABLE IV. Total relaxation energy values (eV) for Cu, Zn, Ga, and Ge for the three main Auger processes. $R(M_{45}M_{45};{}^1G)$ has been obtained from the ^1G final-state term position in the $L_3M_{45}M_{45}$ Auger spectrum. $R(M_{23}M_{45})$ and $R(M_{23}M_{23})$ were deduced from the best correspondence to the overall $L_3M_{23}M_{45}$ and $L_{23}M_{23}M_{23}$ Auger spectra, respectively (see text).

	Cu	Zn	Ga	Ge
$R(M_{45}M_{45};{}^1G)$	19.0±1.0	20.7±1.0	22.2±1.0	23.3±1.0
$R(M_{23}M_{45})$	22.0±1.0	22.3±1.0	23.9±1.0	25.2±1.0
$R(M_{23}M_{23})$	21.3±1.0	20.7±1.0	22.2±1.0	23.3±1.0

TABLE V. Experimental final-state term positions (eV) for the three main *LMM* Auger processes in Cu, Zn, Ga, and Ge. The terms for which no experimental positions are given were too weak for an accurate assignment.

Auger process	Final-state term	Experimental kinetic energy (eV) Cu	Zn	Ga	Ge
$L_3M_{23}M_{23}$	^1D	767.1±0.5	826.8±0.5	890.3±0.5	953.3±1.0
	^3P	773.5±0.5	834.2±0.5	898.1±0.5	962.1±1.0
$L_2M_{23}M_{23}$	^1D	787.1±2.0	849.4±1.0	916.9±1.0	983.8±1.0
	^3P		856.0±0.5	925.5±0.5	990.9±1.0
$L_3M_{23}M_{45}$	^1F	838.5±0.3	904.2±0.3	973.6±0.3	1043.3±0.3
	^3D	846.4±0.3	913.0±0.3	983.4±0.3	1053.9±0.3
$L_2M_{23}M_{45}$	^1F	857.6±0.5	927.2±0.3	1000.3±0.3	1074.4±0.3
	^3D	864.8±0.5	934.2±0.5	1008.6±0.5	1082.4±0.5
$L_3M_{45}M_{45}$	^1S	913.9±0.3	986.7±0.3	1063.1±0.3	
	^1G	918.0±0.1	991.5±0.1	1068.2±0.1	1144.9±0.1
	^3F	920.8±0.1	994.8±0.1	1071.9±0.1	1148.9±0.1
$L_2M_{45}M_{45}$	^1S	934.3±0.3	1010.3±0.3	1089.9±0.3	1170.0±0.3
	^1G	937.9±0.3	1014.5±0.1	1095.1±0.1	1175.9±0.1
	^3F	940.4±0.5	1017.7±0.3	1098.6±0.3	1179.8±0.3

Ga and Ge (as is well known from their XPS spectra the plasmon satellites for Cu and Zn have negligible intensities) and the Auger peaks involving the M_1 level. Because of the presence of all these extra peaks it is not possible to do a detailed fit to the $L_{23}M_{23}M_{23}$ and $L_{23}M_{23}M_{45}$ Auger spectra in a way as was done for the $L_3M_{45}M_{45}$ spectrum of Ga (Fig. 3). However, just as for the $L_3M_{45}M_{45}$ Auger spectra the experimental peak positions of the most prominent lines in the $L_3M_{23}M_{23}$ spectra can be used to determine F^2, which is the only Coulomb integral involved in the peak splittings in this process.[18] Values for this integral together with the calculated free-atom values from Mann[23] are listed in Table II. For the $L_{23}M_{23}M_{45}$ case only the ^1F-^3D term splitting can be determined experimentally. Because the theoretical splitting of these terms is a sum of F^2, G^1, and G^3 integrals[18] and the spin-orbit coupling constant ξ,[27] no explicit values for these integrals can be obtained from the spectrum. However, the theoretical splitting calculated using Mann's integrals[23] is shown to be in very good agreement with experiment (Fig. 4), so we may expect them to be good for this process. In contrast to the F^2 and F^4 values obtained from the $L_3M_{45}M_{45}$ Auger spectra (Table II) the F^2 values for the $L_3M_{23}M_{23}$ spectra (Table II) are much larger than the atomic values. The reason for this is not clear. However, it should be noted that the calculated Coulomb integrals are for the neutral atom. It may be that for the final state with two M_{23} holes the Coulomb integrals are considerably higher because the wave functions are somewhat less extended. At the moment we are more interested in the $L_3M_{45}M_{45}$ Auger process because the interesting physical properties of the transition metals are determined mainly by the $3d$ electrons.

For that purpose we consider the effective Coulomb interaction $U_{\rm eff}$ which we introduced in the theoretical section. For the ^1G final state in the $L_3M_{45}M_{45}$ Auger process it has the form

$$U_{\rm eff}(M_{45}M_{45};{}^1G)=\mathcal{F}(M_{45}M_{45};{}^1G)-R(M_{45}M_{45};{}^1G)\,.$$

In Table VI the values for $\mathcal{F}$ (calculated using Mann's table[23]) and R (from Table IV) are listed. From this table we see that R strongly reduces the Coulomb interaction between the two M_{45} holes. The question now arises as to how much of this reduction is atomic and how much comes from the fact that the atom is in a solid. A straightforward estimate of the atomic part of $R(M_{45}M_{45};{}^1G)$ aside

TABLE VI. Values for the total relaxation energy R, atomic relaxation energy $R_{\rm at}$, calculated atomic Coulomb energy $\mathcal{F}$, and the effective Coulomb energy $U_{\rm eff}$ for the ^1G final-state term in the $L_3M_{45}M_{45}$ Auger process. All values are in eV.

	Cu	Zn	Ga	Ge
$R(M_{45}M_{45};{}^1G)$	19.0	20.7	22.2	23.3
$R_{\rm at}(M_{45}M_{45};{}^1G)$	6.1	6.1	6.2	6.0
$\mathcal{F}(M_{45}M_{45};{}^1G)$	27.0	30.2	33.3	36.2
$U_{\rm eff}(M_{45}M_{45};{}^1G)$	8.0	9.5	11.1	12.9

from the extra-atomic part due to the surrounding atoms and valence electrons can be made by substituting

$$E(L_{23}M_{45}M_{45};{}^1G) = E_M - E_{M^{2+}} + E(L_{23})$$

and

$$E(M_{45}) = E_{M^+} - E_M$$

into Eq. (1), which then leads to

$$R_{\rm at}(M_{45}M_{45};{}^1G) = E_M - E_{M^{2+}} - 2(E_M - E_{M^+}) + \mathfrak{F}(M_{45}M_{45};{}^1G)$$

for this part. Here E_M, E_{M^+}, and $E_{M^{2+}}$ are total energies of the metal in different ionization states and $E(L_{23})$ and $E(M_{45})$ are core-level binding energies. The total energies were calculated using a numerical Hartree-Fock method. For $E_{M^{2+}}$ the ^1G final-state term was taken. The calculations were done on ions stripped off the $4s$ and $4p$ electrons, i.e., for Ge the states (Ar) $3d^{10}$, $3d^9$, and $3d^8$ were calculated. The results are also listed in Table VI. From this table we see that the atomic part $R_{\rm at}$ of the total relaxation energy R is small and almost constant for the four materials, indicating a large contribution coming from the surrounding atoms and valence electrons. The values are in good agreement with the value of 7.2 eV which Weightman *et al.*[9] found for the atomic part of the total relaxation energy (aside from the outer shell) in Se.

As mentioned in the Introduction the size of $U_{\rm eff}$ (also given in Table VI) as compared to the one-electron bandwidth Γ is very important in determining the physical properties of the transition metals and their compounds. If $U_{\rm eff}$ is larger than twice this bandwidth, the two-hole states, where the two holes are on the same atom, will fall outside of the two-hole states where the holes are on different atoms. The result of this is that the material will no longer behave like a one-electron metal and electron correlations will be important As will be shown in a subsequent paper this is also the condition for obtaining atomiclike Auger linewidths. Band effects in the Auger spectra will appear for $U_{\rm eff} \leq 2\Gamma_{M_{45}}$. Since $U_{\rm eff}$ can be determined from the Auger spectra and also the one-electron bandwidth $\Gamma_{M_{45}}$ can be obtained from XPS it is informative to plot $U_{\rm eff}$ and $2\Gamma_{M_{45}}$ versus atomic number, to see where these curves cross. This is shown in Fig. 5 for the metals Fe, Co, Ni, Cu, Zn, Ga, and Ge. The experimental data for Fe, Co, and Ni used to obtain $U_{\rm eff}$ for these metals were determined by us from the x-ray photoelectron and x-ray excited Auger spectra, in the same way as was done for Cu, Zn, Ga, and Ge. The closed circles were obtained from the measurements of Hüfner and Wertheim.[28] Although the $2\Gamma_{M_{45}}$ values are not well defined because of the complicated density of states, we see that these curves cross in the vicinity of Ni.

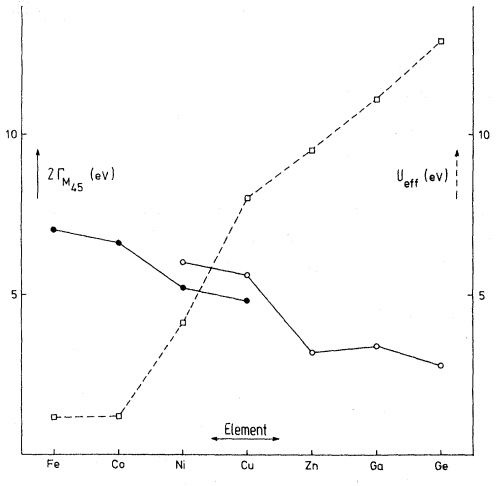

FIG. 5. $U_{\rm eff}$ (squares on dashed line) and $2\Gamma_{M_{45}}$ (circles on solid lines) vs atomic number for Fe, Co, Ni, Cu, Zn, Ga, and Ge in eV. The closed circles were obtained from Ref. 29.

V. CONCLUSIONS

In conclusion we can say that we now understand the *LMM* Auger spectra in Cu, Zn, Ga, and Ge very well and that we are able to obtain from them the relevant effective Coulomb interactions. These Coulomb interactions are strongly reduced from free-atom values by extra-atomic processes, which indicates that the effective on-site Coulomb interaction is strongly dependent on the type of system (i.e. polarizability). The term splittings are on the other hand not as strongly reduced from free-atom values. These results have important consequences in understanding the properties of $3d$ transition metals and their compounds, especially concerning the localized versus itinerant behavior of the $3d$ electrons.

ACKNOWLEDGMENTS

We would like to acknowledge A. Heeres for his experimental assistance and J. Th. van Montfort for computing the total energies of Cu, Zn, Ga, and Ge in different ionization states. This investigation was supported by the Netherlands Foundation for Chemical Research (SON) with financial aid from the Netherlands Organization for the Advancement of Pure Research (ZWO).

APPENDIX

For this appendix we took Ref. 29 as our major source. We start with

$$\omega_{fi} = \left(\frac{2\pi}{\hbar}\right) \left| \int \phi^*_{f(X)} V \phi_i \, d\tau \right|^2 \rho(E_f) . \tag{3}$$

The parameters in this equation have been defined in Sec. III. The two-hole states $\phi_{f(X)}$ and ϕ_i in the LMM Auger transitions can be written

$$\phi_{f(X)} = \psi_{M_b}(1)\psi_{M_c}(2) , \tag{A1}$$

$$\phi_i = \psi_{L_a}(1)\psi_\infty(2) . \tag{A2}$$

Here ψ_{M_b}, ψ_{M_c}, and ψ_{L_a} are bound-state wave functions and ψ_∞ is a continuum wave function. The direct and exchange matrix elements occuring in Eq. (3) can be expressed in Eqs. (A1) and (A2) which leads to

$$D = \int\int \psi_{M_b}(1)\psi_{M_c}(2) \frac{e^2}{|r_1 - r_2|} \psi_{L_a}(1)\psi_\infty(2) \, d\tau_1 \, d\tau_2$$

and

$$E = \int\int \psi_{M_b}(2)\psi_{M_c}(1) \frac{e^2}{|r_1 - r_2|} \psi_{L_a}(1)\psi_\infty(2) \, d\tau_1 \, d\tau_2 .$$

As described in Ref. 29 this can be separated into radial and angular parts.

(a) *Radial matrix elements.* The direct radial elements are of the form

$$D_R(\nu) = e^2 \int\int_{r_1, r_2=0}^{\infty} \gamma_\nu(r_1, r_2) R_{n_b l_b}(r_1) R_{n_c l_c}(r_2) \times R_{n_a l_a}(r_1) R_{\infty l_k}(r_2) r_1^2 r_2^2 \, dr_1 \, dr_2 .$$

Here the $R_{n_a l_a}$, $R_{n_b l_b}$, and $R_{n_c l_c}$ are radial wave functions that describe states characterized by the principal and angular momentum quantum numbers shown as indices where a, b, and c indicate the L_a, M_b, and M_c bound states. $R_{\infty l_k}$ expresses the continuum wave function with angular momentum quantum number l_k and

$$\gamma_\nu(r_1, r_2) = \begin{cases} r_1^\nu / r_2^{\nu+1} , & r_1 < r_2 , \\ r_2^\nu / r_1^{\nu+1} , & r_1 > r_2 . \end{cases}$$

Exchange r_1 and r_2 in the first two R's leads to the radial exchange term $E_R(\nu)$.

(b) *Angular matrix elements.* Because of the large spin-orbit coupling in the L_{23} level (20–30 eV for the elements in concern), the initial two-hole state has to be described in the j-j coupling scheme while the final two-hole state can be represented in LS coupling. The two-hole wave functions in these two representations are

$$\begin{aligned} &\psi(n_a l_a j_a, {}^\infty l_k j_k; JM) \quad j\text{-}j \text{ coupling} , \\ &\psi(n_b l_b, n_c l_c; LSJM) \quad LS \text{ coupling} . \end{aligned} \tag{A3}$$

The j-j wave function (A3) can be expressed in its corresponding LS function by

$$\psi(n_a l_a j_a, {}^\infty l_k j_k; JM) = \sum_{LS} [(2S+1)(2L+1)(2j_a+1)(2j_k+1)]^{1/2} \begin{Bmatrix} \frac{1}{2} & l_a & j_a \\ \frac{1}{2} & l_k & j_k \\ S & L & J \end{Bmatrix} \psi(n_a l_a, {}^\infty l_k; LSJM) ,$$

where

$$\begin{Bmatrix} \frac{1}{2} & l_a & j_a \\ \frac{1}{2} & l_k & j_k \\ S & L & J \end{Bmatrix}$$

is the 9-j symbol. In LS coupling the antisymmetrized and properly normalized two-hole function $\psi(n_b l_b, n_c l_c; LSJM)$ is of the form [$\psi(n_a l_a, {}^\infty l_k; LSJM)$ can be expressed in the same way]:

$$\psi(n_b l_b, n_c l_c; LSJM) = 2^{-1/2} \sum_{M_L M_S} (SM_S LM_L | JM)[\varphi(n_b l_b n_c l_c LM_L) + (-1)^{l_b + l_c - L + S} \varphi(n_c l_c n_b l_b LM_L)] \chi(\tfrac{1}{2}\tfrac{1}{2} SM_S) ,$$

where

$$\varphi(n_\alpha l_\alpha n_\beta l_\beta LM_L) = \sum_{m_\alpha m_\beta} (l_\alpha m_\alpha l_\beta m_\beta | LM_L) \varphi_1(l_\alpha m_\alpha) \varphi_2(l_\beta m_\beta) R_1(n_\alpha l_\alpha) R_2(n_\beta l_\beta)$$

and

$$\chi(\tfrac{1}{2}\tfrac{1}{2} SM_S) = \sum_{m_s m_{s'}} (\tfrac{1}{2} m_s \tfrac{1}{2} m_{s'} | SM_S) \chi_1(m_s) \chi_2(m_{s'}) .$$

Here $\varphi_i(l_j m_j)$, $R_i(n_j l_j)$, and $\chi_i(m_{s'})$ are the one-hole angular, radial and spin-wave functions of hole i, respectively, with quantum numbers n_j, l_j, m_j, and $m_{s'}$. The transition probability as a function of j_a(index a means L_2 or L_3 in our case) and of L, S of the final-state term X now becomes

$$\omega_{j_a LS} = \sum_{j_k} \sum_{J} (2J+1)(2L+1)(2S+1)(2j_a+1)(2j_k+1) \begin{Bmatrix} \frac{1}{2} & l_a & j_a \\ \frac{1}{2} & l_k & j_k \\ S & L & J \end{Bmatrix}^2 \times \sum_{l_k} \left| \frac{1}{\hbar} \left\langle \psi(n_b l_b, n_c l_c; LSJM) \left| \frac{e^2}{r_{12}} \right| \psi(n_a l_a, \infty l_k; LSJM) \right\rangle \right|^2 .$$

Separation into radial and angular factors as discussed before finally leads to

$$\omega_{j_a LS} = \sum_{j_k} \sum_{J} (2J+1)(2L+1)(2S+1)(2j_a+1)(2j_k+1) \begin{Bmatrix} \frac{1}{2} & l_a & j_a \\ \frac{1}{2} & l_k & j_k \\ S & L & J \end{Bmatrix}^2 \sum_{l_k} \left| \frac{1}{\hbar} \sum_{\nu} [d_\nu D_R(\nu) \pm (-1)^{l_b+l_c} e_\nu E_R(\nu)] \right|^2 , \tag{A4}$$

where the (+) sign holds for even $L+S$ and the (−) sign for odd $L+S$. $D_R(\nu)$ and $E_R(\nu)$ are the direct and exchange radial matrix elements mentioned before. The angular factors d_ν and e_ν are

$$d_\nu = (-1)^{l_b+l_c+L} (l_a \| C^\nu \| l_b)(l_k \| C^\nu \| l_c) \begin{Bmatrix} l_a & l_k & L \\ l_b & l_c & \nu \end{Bmatrix}$$

and

$$e_\nu = (-1)^{l_b+l_c+L} (l_a \| C^\nu \| l_c)(l_k \| C^\nu \| l_b) \begin{Bmatrix} l_a & l_k & L \\ l_c & l_b & \nu \end{Bmatrix} .$$

Here $(l_1 \| C^\nu \| l_2)$ is the reduced matrix element of the spherical harmonic multiplied by $[4\pi/(2\nu+1)]^{1/2}$ and

$$\begin{Bmatrix} l_1 & l_2 & L \\ l_3 & l_4 & S \end{Bmatrix}$$

is the 6-j symbol. The values of $D_R(\nu)$ and $E_R(\nu)$ used in our computation are those tabulated by McGuire[22] (Cu and Ga were interpolated). The 3-j, 6-j, and 9-j symbols occurring in Eq. (A4) were calculated using the tables of Rotenberg[30] and Matsunoba *et al.*[31]

[1] G. A. Sawatzky and E. Antonides, J. Phys. Suppl. 37, C4-117 (1976).
[2] J. Hubbard, Proc. R. Soc. A 276, 238 (1963); 277, 237 (1964); 281, 401 (1964).
[3] P. W. Anderson, Phys. Rev. 124, 41 (1961).
[4] N. D. Lang and H. Ehrenreich, Phys. Rev. 168, 605 (1968).
[5] G. M. Stocks, R. W. Williams, and J. S. Faulkner, Phys. Rev. B 4, 4390 (1971).
[6] S. P. Kowalczyk, R. A. Pollak, F. R. McFeely, L. Ley, and D. A. Shirley, Phys. Rev. B 8, 2387 (1973).
[7] C. J. Powell and A. Mandl, Phys. Rev. Lett. 29, 1153 (1972).
[8] L. Yin, T. Tsang, I. Adler, and E. Yellin, J. Appl. Phys. 43, 3464 (1972).
[9] P. Weightman, E. D. Roberts, and C. E. Johnson, J. Phys. C 4, 550 (1975).
[10] E. D. Roberts, P. Weightman, and C. E. Johnson, J. Phys. C 8, 1301 (1975).
[11] R. Hoogewijs, L. Fiermans, and J. Vennik, Chem. Phys. Lett. 38, 471 (1976).
[12] E. D. Roberts, P. Weightman, and C. E. Johnson, J. Phys. C 8, 2336 (1975).
[13] E. D. Roberts, P. Weightman, and C. E. Johnson, J. Phys. C 8, L301 (1975).
[14] S. Aksela, J. Väyrynen, and H. Aksela, Phys. Rev. Lett. 33, 999 (1974).
[15] J. C. Helmer and N. H. Weichert, Appl. Phys. Lett. 13, 266 (1968).
[16] N. Beatham and A. F. Orchard, J. Electron. Spectrosc. Relat. Phenom. 9, 129 (1976).
[17] D. A. Shirley, Phys. Rev. A 7, 1520 (1973).
[18] J. C. Slater, *Quantum Theory of Atomic Structure* (McGraw-Hill, New York, 1960), Vol. 2.
[19] A. de Shalit and I. Talmi, *Nuclear Shell Theory* (Academic, New York, 1963), Chaps. 19–21.
[20] L. I. Yin, I. Adler, M. H. Chen, and B. Crasemann, Phys. Rev. A 7, 897 (1973).
[21] J. A. D. Matthew, J. D. Nuttall, and T. E. Gallon, J. Phys. C 9, 883 (1976).
[22] E. J. McGuire (unpublished).
[23] J. B. Mann, Los Amalos Scientific Laboratory Report No. LASL-3690, 1967 (unpublished).
[24] G. Schön, J. Electron. Spectrosc. Relat. Phenom. 1, 377 (1972/73).
[25] J. E. Castle and D. Epler, Proc. R. Soc. A 339, 49 (1974).
[26] I. Lindau and C. G. Ribbing, Phys. Status Solidi B 59, 259 (1973).
[27] E. U. Condon and G. H. Shortly, *The Theory of Atomic Spectra* (Cambridge U. P., London, 1935).
[28] S. Hüfner and G. K. Wertheim, Phys. Lett. A 47, 349 (1974).
[29] V. O. Kostroun, M. H. Chen, and B. Crasemann, Phys. Rev. A 3, 533 (1971).
[30] M. Rotenberg, *The 3-j and 6-j Symbols* (Lockwood, London, 1959).
[31] H. Matsunoba and H. Takabe, Prog. Theor. Phys. 14, 589 (1955).